






Intra-Data Centre Flexible PAM Transmission System Using an Integrated InP-Si₃N₄ Dual Laser Module

Marcos Troncoso-Costas , *Student Member, IEEE*, Devika Dass , *Student Member, IEEE*,
Colm Browning , *Member, IEEE*, Francisco J. Diaz-Otero, Chris G. H. Roeloffzen ,
and Liam P. Barry , *Senior Member, IEEE*

Abstract—Flexible Pulse Amplitude Modulation (FlexPAM) consists of the use of non-standard PAM formats, such as PAM-5 or PAM-6, to increase the granularity of the link capacity for a given baud rate. In this paper, we demonstrate FlexPAM systems as a scalable solution for future data center interconnects, introduce a symbol-to-bit mapping that minimizes the effect of intensity noise in the performance of non-power of two number of levels formats, and present experimental and simulation results of an unamplified FlexPAM transmission system over 1 km of single-mode fiber. 20 GBaud transmission was successfully demonstrated experimentally for modulation formats ranging from OOK up to PAM-16 using an integrated InP-Si₃N₄ laser. In addition, a simulation to closely replicate the experiment was used to determine the system requirements to achieve transmission rates of up to 200 Gbps on a single wavelength, at a baud rate of 53.5 Gbaud with component bandwidth limitations of 30 GHz.

Index Terms—Data centers, FlexPAM, integrated photonics, PAM-16.

I. INTRODUCTION

THE increasing popularity of online services like streaming platforms, cloud storage, cloud computing, or video call services is driving an unprecedented rise in the bandwidth requirements of data centers (DC). The current trend in intra-DC links consists of moving towards transmission rates up to 100 Gbit/s per wavelength using 4-level pulse amplitude modulation (PAM-4) [1]. The need for increased capacity within the DC can be achieved by increasing the number of lanes (wavelengths),

via wavelength division multiplexing (WDM), or data rate per lane in the intra-DC link. Increasing the data rate per lane can be achieved through the use of more advanced modulation formats with intensity modulation and direct detection (IM/DD) technology, such as PAM-8/16 [2], or an optical coherent approach using complex modulation such as 16-quadrature amplitude modulation (QAM) [3]. As coherent communications technologies become more cost-effective through advances in integrated photonics, it is feasible that a coherent approach may be adopted in future DC networks, however, due to cost issues, it is anticipated that DCs will continue to employ IM/DD in the short to medium term. Increasing the data rate per lane, in an intra-DC link, by moving to higher-order formats beyond PAM-4 will require improved signal-to-noise ratio (SNR), which will place additional limitations on the components used in the transmission system. Works on IM/DD transmissions at rates beyond 100 Gbaud [2], [4] demonstrate that it is feasible to obtain single lane data rates in excess of 200 Gbit/s. However, the transition towards a WDM implementation, in combination with some degree of optical switching (implemented using optical filters and multiplexers) [5]–[7], can result in a drastic variation in path loss present in individual server-to-server links in the DC. This in turn leads to different achievable link data rates, which can be accommodated by operating at a constant baud rate with different modulation formats. With traditional PAM-M formats, where M is a power of two, the SNR requirements grow sharply as the number of levels increases from 4 to 8 and 16, limiting potential capacity increases. This constraint can be alleviated by the use of probabilistic shaping (PS) of high-order traditional PAM-M formats [8], [9], which can potentially give enhanced capacity and performance at the cost of additional computational cost. Another option consists of the use of FlexPAM [10] formats, in which a fractional number of bits is encoded in each symbol by using a non-power of two number of levels (e.g., PAM-6). The use of FlexPAM enables finer granularity in the modulation format that gives the maximum throughput for a specific system SNR (which may change due to temperature variations that alter the laser output power and receiver noise, and different optical paths as optical switching is implemented in future DC architectures) at the very modest computational cost of a lookup table.

Some examples of non-power of two PAM levels can be found in the literature: Ingham *et al.* [11] proposed the use of PAM-3

Manuscript received October 12, 2021; revised November 12, 2021; accepted November 12, 2021. Date of publication November 17, 2021; date of current version December 21, 2021. This work was supported in part by a research Grant from Science Foundation Ireland (SFI) under Grants 18/SIRG/5579, 13/RC/2077-P2, and 12/RC/2276-P2. (*Corresponding author: Marcos Troncoso-Costas.*)

Devika Dass, Colm Browning, and Liam P. Barry are with the School of Electronic Engineering, Dublin City University, Glasnevin, 9 D09 V209 Dublin, Ireland (e-mail: devika.dass2@mail.dcu.ie; colm.browning@dcu.ie; liam.barry@dcu.ie).

Marcos Troncoso-Costas is with the School of Electronic Engineering, Dublin City University, Glasnevin, 9 D09 V209 Dublin, Ireland, and also with the AtlanTTic Research Center, University of Vigo, EI Telecommunication, Campus Universitario s/n, 36310 Vigo, Spain (e-mail: marcos.troncosocostas2@mail.dcu.ie).

Francisco J. Diaz-Otero is with the AtlanTTic Research Center, University of Vigo, EI Telecommunication, Campus Universitario s/n, 36310 Vigo, Spain (e-mail: fjdz@com.uvigo.es).

Chris G. H. Roeloffzen is with the LioniX International BV, 7521 AN Enschede, The Netherlands (e-mail: c.g.h.roeloffzen@lionix-int.com).
Digital Object Identifier 10.1109/JPHOT.2021.3128767

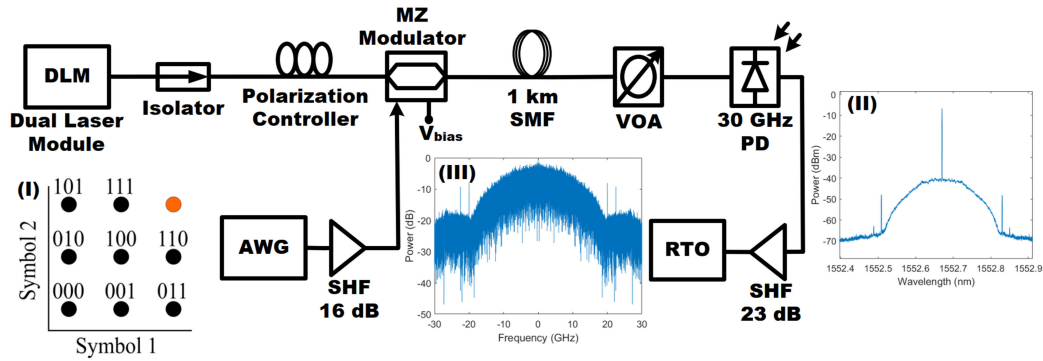


Fig. 1. Experimental setup. The inset (I) shows the asymmetric PAM-3 symbols-to-bit mapping. Inset (II) shows the optical spectrum of a PAM-8 signal at the PD and (III) shows the received electrical spectrum at the RTO.

and compared its performance with on-off keying (OOK) and PAM-4 in a simulation study, while Zhou *et al.* [10], [12] recently studied the theoretical performance of the different PAM levels ranging from PAM-4 to PAM-8 in the context of intra-DC links. Wei *et al.* [13]–[15] demonstrated an experimental comparison between PAM-4, PAM-6, and PAM-8, showing transmission rates over 200 Gbps but relying on the use of complex digital signal processing (DSP) techniques such as a Volterra nonlinear equalizer, which may not be suitable for the existing intra-DC links.

The improvement in SNR required to achieve higher-order modulation formats, as well as increasing transmission distance, is producing a transition towards externally modulated lasers [16] developed using photonic integrated circuit (PIC) technology, which can also provide sources for intra-DC links with lower power consumption and smaller footprint [17]. Moreover, integration in chip with other components such as modulators, amplifiers, or filters can aid the development of fully integrated transceivers for future DC links. In this paper, we present a simulation and an experimental demonstration of a short-reach optical transmission system using FlexPAM formats ranging from OOK to PAM-32. At the transmitter, a photonic integrated dual laser module based on InP semiconductor optical amplifiers (SOA) and low loss Si_3N_4 feedback circuits is used as an optical source. 20 GBaud transmission over 1 km of single-mode fiber (SMF) was demonstrated experimentally for 11 different PAM formats up to PAM-16, achieving a bit error ratio (BER) below 3.8×10^{-3} for 10 formats, including PAM-16. This work harnesses the properties of the laser described in [18] to enable experimental FlexPAM transmission demonstrations and performance analyses aimed at next generation flexible DC environments. In addition, the capabilities of the developed system are further explored through numerical simulations which, under the same conditions and baud rate as the experiment, closely match the experimentally measured results, and show that with an increase of 7 dB on the electrical signal SNR, the system is capable of supporting PAM-32. The simulation also shows that with a 5 dB increase in SNR beyond that used in the experimental work and only a moderate increase in transmitter bandwidth, 53.5 GBaud transmission is feasible for modulation formats up to PAM-16, reaching data rates as high as 214 Gbit/s on a single wavelength.

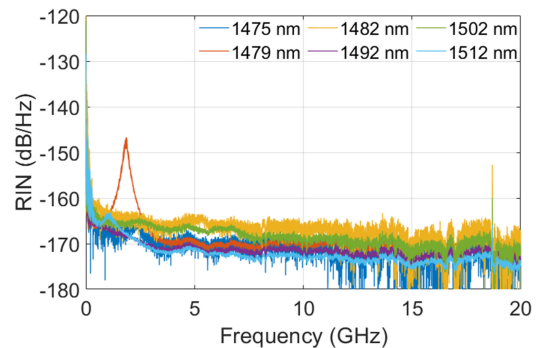


Fig. 2. Measured RIN at different sample wavelengths for the tunable laser module with the gain section biased at 170 mA.

II. INTEGRATED DUAL LASER MODULE

The integrated dual tunable laser module used for the experiment consists of two lasers, each one consisting of an InP gain section and Si_3N_4 phase and cavity sections. The thermo-optically tunable phase sections and the feedback circuits, consisting of two microring resonators (MRR) in a Vernier configuration, create an MRR based external cavity laser, allowing the module to cover a wavelength range of over 100 nm, covering the full C band, most of the S band, and part of the L band. Low loss Si_3N_4 waveguides enable the introduction of long photon lifetimes into the laser resonator, which results in a significant increase of coherence properties, such as spectral coverage and output power with low intensity noise [19]. This device shows values of relative intensity noise (RIN) as low as -165 dB/Hz [20] over the whole spectrum (Fig. 2), which has enabled us to demonstrate IM/DD operation up to PAM-16, and a high side mode suppression ratio (SMSR) of more than 50 dB. To achieve these conditions, over different biases, the different sections of the laser need to be all tuned accordingly, unlike a conventional single section laser where simply increasing the bias current will result in a decrease in the RIN. The advantages of extremely low RIN (well below the typical values of -140 dB/Hz for other available integrated tunable sources [21], [22]) over such a wide range, combined with a small footprint, make the dual tunable laser module a very compelling option for spectrally efficient WDM systems based on IM/DD technology. A more detailed

TABLE I
THEORETICAL AND REAL NUMBER OF BITS PER SYMBOL OBTAINED
FOR EACH PAM LEVEL

M	$\log_2 M$	$NSym$	bits/Sym	DR@20	DR@53.5
2	1	1	1	20	53.5
3	1.59	2	1.5	30	80.25
4	2	1	2	40	107
5	2.32	4	2.25	45	120.375
6	2.59	2	2.5	50	133.75
7	2.81	4	2.75	55	147.125
8	3	1	3	60	160.5
10	3.32	4	3.25	65	173.875
12	3.59	2	3.5	70	187.25
14	3.81	4	3.75	75	200.625
16	4	1	4	80	214

characterization of the device can be found in [18]. For this work, we used a single laser output from the dual laser module, with the wavelength set to 1552.7 nm, an SMSR of more than 50 dB and an output power of +9.7 dBm.

III. SYMBOL-TO-BIT MAPPING

For the standard power of two PAM formats, we used gray encoding to map each symbol to the corresponding bits. The non-standard PAM levels are encoded by grouping them in packets of symbols. Table I shows the maximum achievable bits per symbol ($\log_2 M$) of each PAM level, the number of symbols used for encoding ($NSym$), the bits per symbol (bits/Sym) obtained and the total data rate in Gbit/s of the link when operated at 20 GBaud and at 53.5 GBaud (DR@20 and DR@53.5 respectively). Based on the idea behind PS - where the density of some symbols is reduced to improve performance at the expense of some information per symbol - we defined two different symbol-to-bit mapping techniques: The first one, which is asymmetric, is realized by sorting all possible N -symbol combinations in terms of their total power, with bits assigned in ascending order. Inset (I) of Fig. 1 shows the mapping of symbols to bits of a PAM-3 signal. PAM-5, PAM-7, PAM-10 and PAM-14 mapping follows the same principle on the corresponding 4-symbol combinations. This method ensures a lower density of high power levels, therefore reducing the average power of the signal and improving its performance under low SNR conditions [8], [9], whenever non-standard PAM formats are used. Alternatively, instead of reducing the density of the upper levels on the non-standard PAM formats, the mapping can be optimized for bandwidth-limited systems by removing the sharpest transitions from minimum to maximum (and vice versa), i.e., reducing the density of upper and lower levels symmetrically, resulting in a symbol distribution similar to the PS-PAM-16 demonstrated in [4]. Fig. 3 shows an example of the probability distribution of each level in a PAM-12 sequence, when reducing the density of higher levels (asymmetric) and when removing the sharp transitions (symmetric).

The main drawback associated with the use of non-standard PAM formats is that, as the modulation format increases, the complexity of the bit mapping increases rapidly (especially with a high number of encoding symbols). This makes some of the

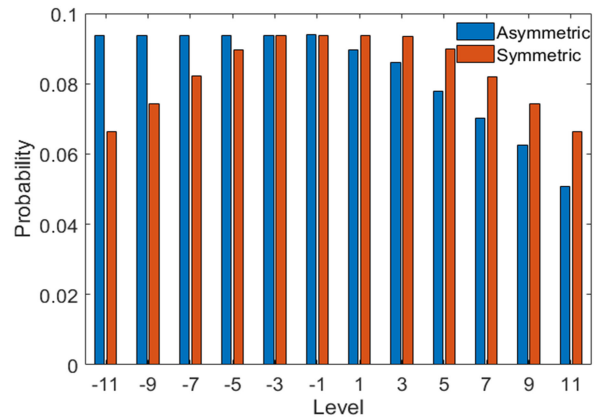


Fig. 3. Probability per symbol on a PAM-12 signal using symmetric and asymmetric encoding.

modulation formats less appealing for their use in intra-DC links due to an increased latency at the decoding step (e.g., PAM-14 requires the mapping of 15 bits into $14^4 = 38416$ symbol combinations).

IV. EXPERIMENTAL SETUP

The experiment was performed using the setup shown in Fig. 1. A pseudorandom multilevel sequence of 2^{15} symbols was generated offline for each PAM level using MATLAB, and pre-distorted to compensate for the nonlinear transfer function of the LiNbO₃ Mach-Zehnder modulator (MZM) from Sumitomo (40 Gbit/s MZM). Even though a discrete MZM was used for this experiment, integrated technologies currently available [23] can enable the use of fully integrated transmitter solutions in short reach links. Asymmetric symbol-to-bit mapping was used for the non-standard PAM signals. The 20 Gbaud signals were generated using an arbitrary waveform generator (AWG) (3-dB bandwidth of 33 GHz) operating at 90 GSa/s. A 16 dB gain electrical amplifier (3-dB bandwidth of 25 GHz) was placed before the MZM to match its V_π of ~ 2.3 V. After transmission over 1 km of SMF, a variable optical attenuator (VOA) was used to sweep the received optical power (ROP) falling on the photodetector (PD) (3-dB bandwidth of 30 GHz). A 23 dB gain electrical amplifier (3-dB bandwidth of 55 GHz) was used before the signal was captured for offline processing with a real-time oscilloscope (RTO) (3-dB bandwidth of 110 GHz) operating at a sample rate of 256 GSa/s.

The DSP performed on the received signals consisted of matched filtering with a 20 GHz root-raised-cosine (RRC) filter, resampling, synchronization, adaptive equalization, and decoding. The normalization of the non-power of two PAM formats was performed considering the mean and standard deviation expected from the non-uniform probability distribution of the symbols. A decision-directed least-mean-square (DD-LMS) algorithm was used for updating the weights of the 13-tap linear equalizer. The bit error ratio (BER) was calculated by counting errors over several captured sequences.

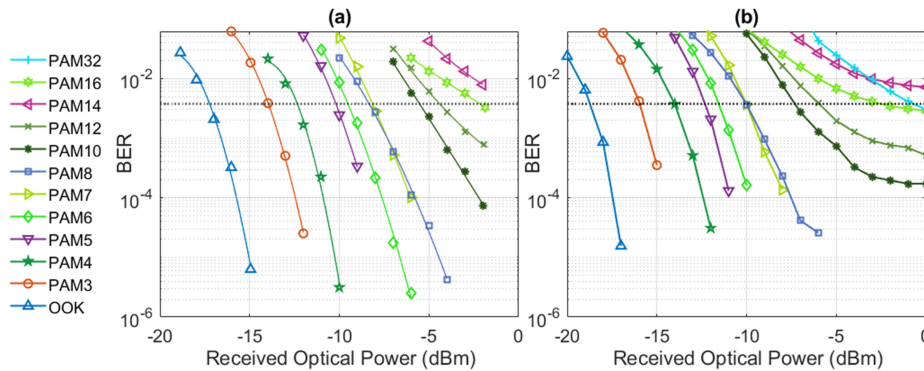


Fig. 4. (a) Experimental results of BER vs. ROP of 20 GBaud transmission using various modulation formats ranging from OOK to PAM-16 after 1 km of SMF. (b) Simulation results of BER vs. ROP of 20 GBaud transmission using various modulation formats ranging from OOK to PAM-32 after 1 km of SMF. Electrical SNR of 27 dB from OOK to PAM-16, and 34 dB for PAM-32. Asymmetric mapping was used for the non-standard formats.

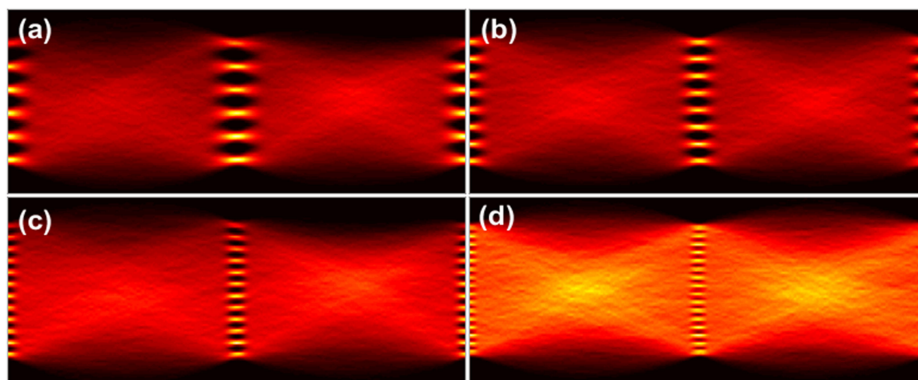


Fig. 5. (a) PAM-6 at ROP -7 dBm, (b) PAM-8 at ROP -4 dBm, (c) PAM-12 at ROP -2 dBm, (d) PAM-16 at ROP -2 dBm. It can be noticed how the upper levels on (a) and (c) are less densely populated due to the asymmetric mapping used.

V. SIMULATION

A simulation was developed in Matlab for modelling the full system shown in Fig. 1. To compare its performance with the measurements from the experiment, the 3-dB simulation bandwidth value of all electrical and optoelectronic components was set to the corresponding experimental value. The laser's RIN was set to -160 dB/Hz, and the sampling frequencies of AWG and RTO were set to 90 GSa/s and 256 GSa/s respectively. The SNR of the electrical signal driving the MZM was set to 27 dB, the value at which the simulation results closely match those observed from the experiment. This SNR accounts for both the noise of the AWG and the electrical amplifier, as well as any degradation produced by nonlinear distortions, quantization noise and other interactions.

A comparison between the symmetric and asymmetric mapping techniques was performed using 20 Gbaud transmission with the same conditions as the experiment.

VI. RESULTS

The experimental performance of each PAM level in the unamplified system was compared in terms of BER vs. ROP. The results after 1 km of SMF (Fig. 4(a)) achieve performance below the 7% overhead forward error correction (FEC) limit for all modulation formats except PAM-14. Fig. 5(a)-(d) show the

eye diagrams corresponding to PAM-6, PAM-8, PAM-12, and PAM-16 signals. PAM-16 reaches below FEC performance at ROP of -2 dBm, resulting in a receiver sensitivity penalty of 15 dB compared to OOK. Even though lower order modulation formats are less affected by the SNR of the system, it can be seen that PAM-7 performs similarly to PAM-8, and PAM-14 worse than PAM-16. This is a result of the additional penalty introduced by the symbol-to-bit mapping, where standard PAM formats can take advantage of gray encoding, while non-standard formats suffer from the fact that the encoding is performed in blocks of multiple symbols. In the latter case, a decision error produces a cascading effect in which bits corresponding to the whole block of symbols are affected. This becomes more significant as the number of symbols used for decoding increases, and leads to the previously mentioned behavior of PAM-7 and PAM-14, where a 4-symbol format is adjacent to a standard PAM format (PAM-8 and PAM-16 respectively).

Fig. 4(b) shows the results of the 20 GBaud simulation with an electrical SNR of 27 dB on the driving currents operating from OOK up to PAM-16. The figure shows how the trend of the simulated results closely resembles that of the experimental measurements. However, a difference in performance between experiment and simulation of up to 2 dB at the FEC threshold, can be observed for lower-order modulation formats at lower ROPs. This difference in performance - which increases as

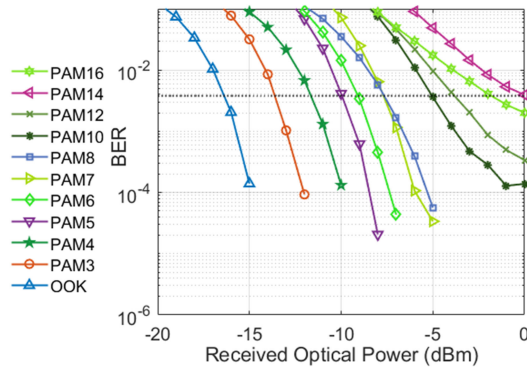


Fig. 6. Simulation results of BER vs. ROP of 53.5 GBaud transmission using various modulation formats ranging from OOK to PAM-16 after 1 km of SMF. Electrical SNR of 32 dB. Asymmetric mapping was used for the non-standard formats.

the number of levels decreases from PAM-12 down to OOK - can be attributed to the power-dependent noise figure of the electrical amplifier at the receiver for lower ROPs, which was not accounted for in the simulation. Additionally, in order to analyze the system’s performance if lower noise AWG and RF amplifiers were available, the value of the SNR was increased. The system was found to support PAM-32, with performance below the FEC limit obtained for an enhanced electrical SNR of 34 dB.

The simulation was also carried out with a PAM baud rate of 53.5 Gbaud and an electrical SNR of 32 dB (5 dB higher than what was used for the base simulation, and which may be achieved by using a low drive voltage modulator [23] driven directly by the AWG). All electrical bandwidths in the system were set to 30 GHz, and a sampling rate of 107 GSa/s was set for both AWG and RTO. The RRC filter bandwidth at the DSP side was also set to 30 GHz. Under these conditions (Fig. 6), performance below FEC was achieved for PAM-16 at -2 dBm, providing a total transmission capacity of 214 Gbps. A receiver sensitivity penalty of up to 2 dB can be observed at the FEC limit for OOK with respect to the 20 Gbaud simulation (OOK curves from Fig. 4(b) and 6). This penalty is reduced as the modulation format increases, indicating how the choice of modulation format dictates whether system performance is ultimately limited by bandwidth or SNR. The ROP required to achieve below FEC limit performance in the experiment, the 20 Gbaud simulation and the 53.5 Gbaud simulation, can be seen in Fig. 7.

Comparing the performance of symmetric and asymmetric mapping of non-standard PAM formats at 20 Gbaud (Fig. 8), it can be seen how the asymmetric encoding gives a marginal gain at low-order modulation formats, while no noticeable difference is observed at the higher-orders. Since higher-order formats are more dependent on the SNR, and the asymmetric mapping is expected to perform better in the presence of increased system noise, it can be concluded that the performance gain is small and may be negligible given the level of noise fluctuations in the systems.

The effects of RIN in the system’s performance were studied by measuring the receiver sensitivity penalty at the FEC limit

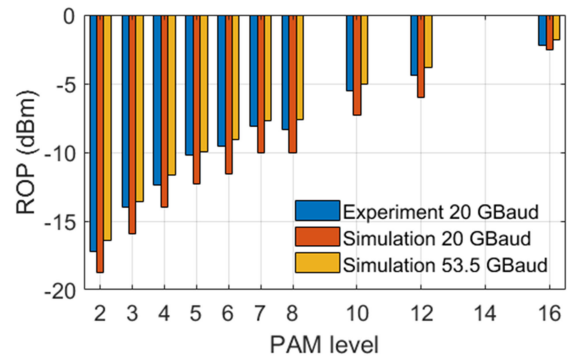


Fig. 7. Received optical power required to achieve below FEC performance for each PAM level according to the experimental results, the 20 Gbaud simulation and the 53.5 Gbaud simulation. Missing values at PAM-14 correspond to the system not reaching the FEC limit.

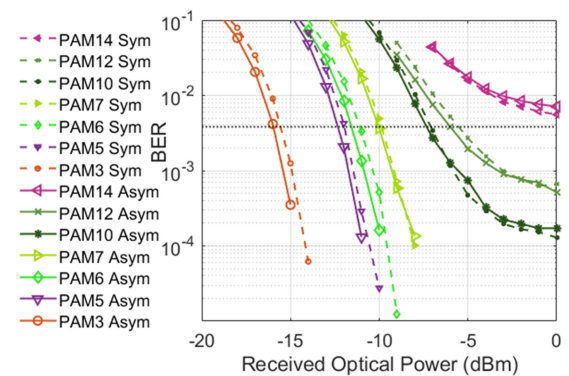


Fig. 8. Asymmetric and symmetric simulation results of BER vs. ROP of 20 GBaud transmission using non-standard PAM formats ranging from PAM-3 to PAM-14 after 1 km of SMF. Electrical SNR of 27 dB.

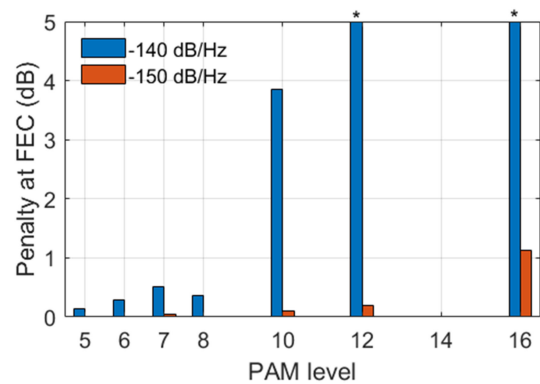


Fig. 9. Receiver sensitivity penalty at the FEC limit for different PAM levels for the 20 Gbaud simulation. Missing values at PAM-14 correspond to the system not reaching the FEC limit. (*) PAM-12 and PAM-16 do not reach the FEC limit at a RIN value of -140 dB/Hz.

for the 20 Gbaud simulation with a RIN of 140 dB/Hz and -150 dB/Hz with respect to the original results (-160 dB/Hz). As it can be seen in Fig. 9, a power penalty of over 1 dB was obtained for PAM-16 for RIN value of -150 dB/Hz, but minimal differences can be seen at lower-order formats. At -140 dB/Hz significant degradations can be seen, and only modulation formats below PAM-10 reach FEC limit performance.

VII. CONCLUSION

Bandwidth requirements are causing constant capacity increases in DCs, and considering cost issues, formats compatible with IM/DD are expected to remain in place as the main schemes for short-reach communications in intra-DC links in the short to medium term. FlexPAM modulation formats provide finer data rate granularity and improved flexibility, which can help to maximize the capacity of a system subject to variable noise and/or optical path differences in an optically switched environment. An asymmetric symbol-to-bit mapping and encoding were proposed and demonstrated for the non-power of two PAM formats that minimize the density of high power symbols, and should help mitigate the effects of increased noise in the performance. The mapping was performed with a generic algorithm, but better results may be achieved by tailoring a different mapping, with a lower average bit difference between adjacent symbols, for each non-power of two PAM format. A symmetric symbol-to-bit mapping that minimizes the number of sharp transitions between the edge levels was also proposed and compared on a simulation basis, and even though no conclusive results were obtained, further research is needed to compare both techniques on more diverse situations.

This work has presented, for the first time to the best of our knowledge, an experimental demonstration of a short reach unamplified transmission system with a transmission rate granularity down to 0.25 bits per symbol ranging from OOK up to PAM-16. The extremely low RIN of the integrated laser allowed for below FEC performance for modulation formats up to PAM-16 with reduced DSP complexity compared to that of previous FlexPAM experimental demonstrations, making it especially suitable for intra-DC links. The experiment was performed at a wavelength of 1552.7 nm, but given the results shown in [18] with the same dual laser module, it can be expected to work similarly over the full 100 nm range covered by the device. Additionally, we were able to show through simulation the feasibility of fulfilling the current standards for 100 Gbit/s, using a 53.5 GBaud PAM-4 signal, with ROPs as low as -11 dBm, as well as a potential transmission capacity of up to 200 Gbps per wavelength, given a modest increase in transmitter bandwidth and a 5 dB SNR increase in our simulation, which could enable Tbit/s DC links using integrated multi-wavelength transmitters. These results show FlexPAM is a suitable option to maximize transmission rates of WDM-based intra-DC links with optical switching and variable path losses.

ACKNOWLEDGMENT

The authors would like to thank KEYSIGHT for letting us use their oscilloscope UXR1104A for this experiment.

REFERENCES

- [1] *IEEE Standard for Ethernet - Amendment 11, 802.3cu-2021, Physical Layers and Management Parameters for 100 Gb/s and 400 Gb/s Operation over Single-Mode Fiber at 100 Gb/s per Wavelength*, IEEE Std. 802.3cu-2021. doi: [10.1109/IEEESTD.2021.9381783](https://doi.org/10.1109/IEEESTD.2021.9381783).
- [2] S.-B. Hossain *et al.*, "Single-Lane 402 Gb/s PAM-8 IM/DD transmission based on a single DAC and an O-Band commercial EML," in *Proc. Optoelectron. Commun. Conf.*, Jul. 2021, pp. 1–4.

- [3] Y. Yue, Q. Wang, and J. Anderson, "Experimental investigation of 400 Gb/s data center interconnect using unamplified high-baud-rate and high-order QAM single-carrier signal," *Appl. Sci.*, vol. 9, no. 12, Jun. 2019, Art. no. 2455, doi: [10.3390/app9122455](https://doi.org/10.3390/app9122455).
- [4] X. Chen *et al.*, "Single-Wavelength and single-photodiode 700 Gb/s entropy-loaded PS-256-QAM and 200-GBaud PS-PAM-16 transmission over 10-km SMF," in *Proc. Eur. Conf. Opt. Commun.*, Brussels, Belgium, Dec. 2020, pp. 1–4, doi: [10.1109/ECOC48923.2020.9333201](https://doi.org/10.1109/ECOC48923.2020.9333201).
- [5] O. Liboiron-Ladouceur, I. Cerutti, P. G. Raponi, N. Andriolli, and P. Castoldi, "Energy-Efficient design of a scalable optical multiplane interconnection architecture," *IEEE J. Select. Top. Quantum Electron.*, vol. 17, no. 2, pp. 377–383, Mar. 2011, doi: [10.1109/JSTQE.2010.2049733](https://doi.org/10.1109/JSTQE.2010.2049733).
- [6] K. Sato, H. Hasegawa, T. Niwa, and T. Watanabe, "A large-scale wavelength routing optical switch for data center networks," *IEEE Commun. Mag.*, vol. 51, no. 9, pp. 46–52, Sep. 2013, doi: [10.1109/MCOM.2013.6588649](https://doi.org/10.1109/MCOM.2013.6588649).
- [7] D. D. Le, L. P. Barry, D. C. Kilper, P. Perry, J. Wang, and C. McArdle, "AgileDCN: An agile reconfigurable optical data center network architecture," *J. Lightw. Technol.*, vol. 38, no. 18, pp. 4922–4934, Sep. 2020, doi: [10.1109/JLT.2020.2999778](https://doi.org/10.1109/JLT.2020.2999778).
- [8] X. Han and I. B. Djordjevic, "Probabilistically shaped 8-PAM suitable for data centers communication," in *Proc. 20th Int. Conf. Transparent Opt. Netw.*, Bucharest, Romania, Jul. 2018, pp. 1–4, doi: [10.1109/ICTON.2018.8473738](https://doi.org/10.1109/ICTON.2018.8473738).
- [9] A. Amari and A. Richter, "Probabilistic shaping for PAM-8 optical ethernet systems," in *Proc. 22nd Int. Conf. Transparent Opt. Netw.*, Bari, Italy, Jul. 2020, pp. 1–4, doi: [10.1109/ICTON51198.2020.9203547](https://doi.org/10.1109/ICTON51198.2020.9203547).
- [10] X. Zhou, R. Urata, and H. Liu, "Beyond 1 Tb/s intra-data center interconnect technology: IM-DD OR coherent?," *J. Lightw. Technol.*, vol. 38, no. 2, pp. 475–484, Jan. 2020, doi: [10.1109/JLT.2019.2956779](https://doi.org/10.1109/JLT.2019.2956779).
- [11] J. D. Ingham, R. V. Penty, I. H. White, and D. G. Cunningham, "Gb/s unequalized PAM3 modulation of an 850 nm VCSEL for next-generation data-communication links," in *Proc. Conf. Lasers Electro-Opt.*, San Jose, CA, USA, 2012, Art. no. CTh3C.4, doi: [10.1364/CLEO_SI.2012.CTh3C.4](https://doi.org/10.1364/CLEO_SI.2012.CTh3C.4).
- [12] X. Zhou, R. Urata, and H. Liu, "Beyond 1Tb/s datacenter interconnect technology: Challenges and solutions (Invited)," in *Proc. Opt. Fiber Commun. Conf.*, San Diego, CA, USA, 2019, Art. no. Tu2F.5, doi: [10.1364/OFC.2019.Tu2F.5](https://doi.org/10.1364/OFC.2019.Tu2F.5).
- [13] J. Wei *et al.*, "Experimental demonstration of advanced modulation formats for data center networks on 200 Gb/s lane rate IMDD links," *Opt. Exp.*, vol. 28, no. 23, Nov. 2020, Art. no. 35240, doi: [10.1364/OE.409905](https://doi.org/10.1364/OE.409905).
- [14] T. Wettlin, S. Calabrò, T. Rahman, J. Wei, and S. Pachnicke, "DSP for high-speed short-reach IM/DD systems using PAM," *J. Lightw. Technol.*, vol. 38, no. 24, pp. 6771–6778, Dec. 2020.
- [15] J. Wei, L. Zhang, C. Prodanic, N. Stojanović, and C. Xie, "Linear pre-equalization techniques for short reach single lambda 225 Gb/s PAM IMDD systems," in *Proc. Eur. Conf. Opt. Commun.*, Sep. 2018, pp. 1–3, doi: [10.1109/ECOC.2018.8535347](https://doi.org/10.1109/ECOC.2018.8535347).
- [16] F. Chang and S. Bhoja, "New paradigm shift to PAM4 signalling at 100/400G for cloud data centers: A performance review," in *Proc. Eur. Conf. Opt. Commun.*, Sep. 2017, pp. 1–3, doi: [10.1109/ECOC.2017.8346164](https://doi.org/10.1109/ECOC.2017.8346164).
- [17] Z. Zhou, R. Chen, X. Li, and T. Li, "Development trends in silicon photonics for data centers," *Opt. Fiber Technol.*, vol. 44, pp. 13–23, Aug. 2018, doi: [10.1016/j.yofte.2018.03.009](https://doi.org/10.1016/j.yofte.2018.03.009).
- [18] D. Dass *et al.*, "28 GBd PAM-8 transmission over a 100 nm range using an InP-Si₃N₄ based integrated dual tunable laser module," *Opt. Exp.*, vol. 29, no. 11, May 2021, Art. no. 16563, doi: [10.1364/OE.421929](https://doi.org/10.1364/OE.421929).
- [19] K.-J. Boller *et al.*, "Hybrid integrated semiconductor lasers with silicon nitride feedback circuits," *Photonics*, vol. 7, no. 1, Dec. 2019, Art. no. 4, doi: [10.3390/photonics7010004](https://doi.org/10.3390/photonics7010004).
- [20] J. P. Epping *et al.*, "Hybrid integrated silicon nitride lasers," in *Proc. Phys. Simul. Optoelectron. Devices XXVIII*, San Francisco, CA, USA, Mar. 2020, Art. no. 56, doi: [10.1117/12.2552264](https://doi.org/10.1117/12.2552264).
- [21] T. Wipiejewski *et al.*, "Performance and reliability of widely tunable laser diodes," in *Proc. 53rd Electron. Compon. Technol. Conf.*, 2003, New Orleans, LA, USA, 2003, pp. 789–795, doi: [10.1109/ECTC.2003.1216376](https://doi.org/10.1109/ECTC.2003.1216376).
- [22] CW Tunable Laser – Butterfly Package | II-VI Incorporated, Accessed: Nov. 11, 2021, [Online]. Available: <https://ii-vi.com/product/cw-tunable-laser-butterfly-package/>
- [23] C. Wang *et al.*, "Integrated lithium niobate electro-optic modulators operating at CMOS-compatible voltages," *Nature*, vol. 562, no. 7725, pp. 101–104, Oct. 2018, doi: [10.1038/s41586-018-0551-y](https://doi.org/10.1038/s41586-018-0551-y).